

## RESSALVA

Atendendo solicitação da autora, o texto completo desta dissertação será disponibilizado somente a partir de 27/03/2020.

UNESP – Universidade Estadual Paulista “Júlio de Mesquita Filho”

Instituto de Química de Araraquara

*Beatriz Lucas Garrote*

***The potentiality and limitations of electrochemical  
impedance spectroscopic methods for molecular  
film applications***

**Araraquara**

**2018**

Beatriz Lucas Garrote

***The potentiality and limitations of electrochemical impedance spectroscopic methods for molecular film applications***

Thesis submitted to post-graduation program from University of São Paulo “Julho de Mesquita Filho” (UNESP, Brazil) in part fulfillment of the requeriment for the degree of Master in Biotechnology.

Supervisor: Prof. Dr. Paulo Roberto Bueno

Co-supervisor: Dr. Flávio Cesar Bedatty

Araraquara  
2018

Beatriz Lucas Garrote

***Potencial e limitações dos métodos de espectroscópicos de impedância eletroquímica em aplicações para filmes moleculares.***

Dissertação apresentada ao Instituto de Química, Universidade Estadual Paulista “Julho de Mesquita Filho” (UNESP) como parte dos requisitos para obtenção do título de Mestre em Biotecnologia.

Orientador: Prof. Dr. Paulo Roberto Bueno  
Coorientador: Dr. Flávio Cesar Bedatty

Araraquara  
2018

FICHA CATALOGRÁFICA

L933p Lucas Garrote, Beatriz  
The potentiality and limitations of electrochemical impedance spectroscopy methods for molecular film applications = Potencial e limitações dos métodos de espectroscópicos de impedância eletroquímica em aplicações para filmes moleculares / Beatriz Lucas Garrote. – Araraquara: [s.n.], 2018  
75 p.: il.

Dissertação (mestrado) – Universidade Estadual Paulista, Instituto de Química  
Orientador: Paulo Roberto Bueno  
Coorientador: Flávio Cesar Bedatty

1. Biossensores. 2. Análise eletroquímica.  
3. Espectroscopia de impedância. 4. Proteínas. 5. Peptídeos.

I. Título

CERTIFICADO DE APROVAÇÃO

TÍTULO DA DISSERTAÇÃO: "The potentiality and limitations of electrochemical impedance spectroscopic methods for molecular film applications"

AUTORA: BEATRIZ LUCAS GARROTE

ORIENTADOR: PAULO ROBERTO BUENO

COORIENTADOR: FLÁVIO CESAR BEDATTY FERNANDES

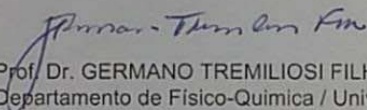
Aprovada como parte das exigências para obtenção do Título de Mestra em BIOTECNOLOGIA, pela Comissão Examinadora:



Prof. Dr. PAULO ROBERTO BUENO  
Departamento de Físico-Química / Instituto de Química - UNESP - Araraquara



Prof. Dr. ASSIS VICENTE BENEDETTI  
Departamento de Físico-Química / Instituto de Química - UNESP - Araraquara



Prof. Dr. GERMANO TREMILOSIO FILHO  
Departamento de Físico-Química / Universidade de São Paulo - USP - São Carlos

Araraquara, 27 de março de 2018

# ***CURRICULUM VITAE***

## **PERSONAL INFORMATION**

Name: Beatriz Lucas Garrote

Birth date: 16/09/1993 – Cieza (Murcia) – Spain

Nacionality: Spanish

Professional address: Institute of Chemistry, Univ. Estadual Paulista (UNESP, São Paulo State University). R. Prof. Francisco Degni, 55. Quitandinha – Araraquara – CEP: 14800-900, São Paulo, Brasil.

## **EDUCATION**

- Degree in biotechnology (2011 – 2015). Completed in *Universitat Politècnica de València*, Valencia (Spain).
- Master of biotechnology (2016 – 2018), at *Universidade Estadual Paulista “Júlio de Mesquita Filho”*, Araraquara (São Paulo, Brazil).

## **INTERSHIP, SCOLARCHIP AND RESEARCH PROJECTS**

- Internship in *Centro de Investigación Príncipe Felipe*, Valencia (Spain) (06/2014 – 07/2014) at the Molecular and Cellular Pathology of Alcohol laboratory.
- Scholarship from the Spanish Government. Completed in Chemistry Department of *Universitat Politècnica de València*, Valencia (Spain) (01/2015 – 09/2015) at the Interuniversity Research Institute for Molecular Recognition and Technological Development (IDM). Project: Strategies for the direct detection of specific sequences of genomic DNA in polymeric surfaces.
- Scholarship from FAPESP (São Paulo, Brazil) for Master development. It was completed at the Physical-Chemistry Department of *Universidade Estadual Paulista “Júlio de Mesquita Filho”* at the Nanobionics Group. Project: The potentiality and limitations of electrochemical impedance spectroscopic methods for molecular film applications.

## **CONFERENCES AND PUBLICATIONS**

- IX International workshop on sensors and molecular recognition (2015) in Valencia (Spain).
- LUCAS-GARROTE, B.; MORAIS, S.; MAQUIEIRA, A. Dual signal amplification for highly sensitive hybridization microassays on chemically activated surfaces. **Sensors and Actuators B: Chemical**, v. 246, p. 1108 – 1115, 2017.

*A mi madre, M<sup>a</sup> Carmen; a mi padre, J. Antonio; a mi hermana, Irene; y a mi hermano, Alejandro.*



# ACKNOWLEDGEMENTS

I would like to thank my supervisor Prof. Paulo Bueno for the support and the guidance, during these two years.

I would like to acknowledge my co-supervisor Dr. Flávio Bedatty for the support, the scientist discussions and the guidance through the experimental difficulties.

I want to recognize the support and collaboration of my colleagues from Nanobionics, in special Dr. Adriano Santos, Ms. Juliana Cecchetto, Raphael Mazzine and Fernanda Bernardo for the hours spent at the lab, discussing, learning and working together.

I gratefully acknowledge the financial assistance of FAPESP (grant n° 2015/17332-1).

I also would like to thank the Chemistry Institute for the facilities and the administrative personnel from the post-graduation section and from the LIEC.

À minha companheira Gabriela Santos, pelo apoio incondicional, a força, o carinho e o amor. Por me fazer sentir em casa. Esse é só o começo de uma longa viagem.

À minha família brasileira, Isabele e Luisa, por ter ocupado o papel de mãe, pai, irmã e amiga nos momentos que mais precisei.

A mis padres, M<sup>a</sup> Carmen y J. Antonio, a mi hermana Irene y a mi hermano Alejandro por haceros sentir tan cerca a 8000 km de distancia.

# Abstract

Biomedicine research is directing its effort to achieve fast, simple, point-of-care analytical devices for disease diagnostic. Label-free electrochemical biosensors based on electrochemical impedance spectroscopy (EIS) are an interesting tool for this purpose. For analytical objective, EIS is more sensitive than other electrochemical techniques, such as amperometric, potentiometric or voltammetry. EIS measures the complex resistance of the system. In faradaic EIS system, variations on the electrode surface are monitored by the charge transfer resistance ( $R_{ct}$ ), so correlations between the variation in  $R_{ct}$  value and the concentration of a specific target could be made. Thus, EIS is a widely used technique for biosensing. Here, an EIS based system for the detection of the protein interleukin-6 (IL-6) was proposed. The working electrode was modified with a self-assembled monolayer (SAM) of alkanethiols, in which the biological receptor (Ab IL-6) was covalently immobilized. During the development of the system experimental problems compromised the analytical response. It was analysed every step of the biosensor construction. It was concluded that defects or pinholes on the SAM were the responsible for the absence of response, since EIS is a technique based on charge transfer and the presence of pinholes on the self-assembled monolayer could allow to free ionic and/or electronic migration. Because of this, it was proposed a second system for IL-6 detection based on electrochemical capacitance spectroscopy (ECS) and using a redox peptide SAM. Again, the sensitive of the system was not high enough to the protein detection. According to previous work published by our group, it was possible to correlate the sensitivity of the system with the molecular weight of the biological receptor and the specific target. It was shown that systems with bigger specific target and similar receptors resulted in more sensitive devices. Moreover, it was observed that system with small receptors and bigger targets showed higher sensitivity. IL-6 is a 26 kDa protein and is the smaller protein tested in an ECS based system by our group, and the biological receptor of the system was an antibody (150 kDa), 5.8 times higher than the biological receptor. Thus, the absence of response of the ECS system was attributed to the small molecular weight of the IL-6 protein and the high difference in weight between the biological receptor and the target.

At the same time, it was performed a preliminary electrochemical study of a system with a redox probe confined on the electrode surface and a second one in solution. The objective was study the signal amplifier behaviour observed when two redox probes are

involved on the system and understand the electrochemical process. It was observed the variation from a capacitive-based system, with the confined redox probe, to an impedance one, when the redox probe in solution was present. The presence of two redox probes decreased the redox capacitance of the electroactive film and the resonance resistance of the electrons between the electrode surface and the film; moreover, increased the energy of the system and the frequency of relaxation, due to the increase of the electron diffusion with the solution.

# Resumo

A pesquisa em biomedicina está direcionando seus esforços para conseguir desenvolver dispositivos analíticos rápidos, simples e *point-of-care* para o diagnóstico de doenças. Os biossensores eletroquímicos *label-free* baseados na espectroscopia de impedância eletroquímica (EIE) são uma ferramenta interessante para este fim. EIE é uma técnica mais sensível do que outras técnicas eletroquímicas, como as amperométricas, potenciométricas ou voltamétricas. Em um sistema EIE com configuração faradaica, as variações na superfície do eletrodo são monitoradas, geralmente, pela resistência de transferência de carga ( $R_{ct}$ ) e pode-se correlacionar as variações no valor do  $R_{ct}$  com a concentração do analito específico. Assim, EIE é uma técnica muito usada para biossensoriamento. Neste trabalho foi proposto um sistema baseado em EIE para a detecção da proteína interleukina-6 (IL-6). O eletrodo de trabalho foi modificado com uma monocamada auto-organizada (SAM) de alcanotióis. Nela é imobilizado covalentemente o receptor biológico (Ab IL-6). Durante o desenvolvimento do trabalho, foram enfrentados alguns problemas experimentais que comprometeram a resposta analítica do sistema. Para encontrar a causa da falta de resposta, foi analisado cada etapa de construção do biossensor. Após esses estudos foi concluído que as razões da ausência de resposta eram os defeitos ou *pinholes* presentes na SAM, devido ao fato de que EIE é uma técnica baseada na transferência de carga e a presença de defeitos na monocamada pode facilitar a migração iônica e/ou eletrônica. Para resolver isso, foi proposto um segundo sistema para a detecção da proteína IL-6 baseado na ECE (espectroscopia de capacitância eletroquímica), usando uma monocamada auto-organizada formada por um peptídeo redox. De novo, a sensibilidade do sistema não foi suficiente para a detecção da proteína. De acordo com trabalhos publicados previamente pelo nosso grupo de pesquisa, foi possível estabelecer uma correlação entre a sensibilidade do sistema e o peso molecular do antígeno e do receptor biológico. Assim, foi observado que sistemas similares mostram maior sensibilidade quanto maior é o analito. Da mesma forma, foi observado que sistemas com receptores biológicos pequenos e analitos maiores mostram maior sensibilidade. Essas duas afirmações podem ter afetado a sensibilidade do sistema proposto, pois a proteína IL-6 é uma proteína de 26 kDa e é a menor proteína já testada pelo nosso grupo em um sistema ECE e o receptor biológico foi um anticorpo de 150 kDa, 5,8 vezes maior do que o analito. Paralelamente, foi realizado um estudo eletroquímico preliminar de um sistema com duas sondas redox, em solução e confinada

na superfície. O objetivo foi estudar o fenômeno de amplificação de sinal observado quando ambas as sondas redox formam parte do sistema e entender o processo eletroquímico. Foi observada uma transformação de um sistema capacitivo, quando só a sonda redox confinada na superfície está presente para um sistema impedimétrico, quando a sonda redox em solução participa no processo. A presença das duas sondas redox diminuiu a capacitância redox da monocamada eletroativa e a resistência de ressonância e aumentou a energia do sistema e a frequência de relaxação, devido a que foi favorecido a difusão dos elétrons com a solução.

# Resumo expandido

Nos últimos anos, o desenvolvimento de metodologias analíticas rápidas e simples para o diagnóstico de doenças tem sido o principal desafio da pesquisa em diagnóstico clínico. Com este objetivo estão sendo usadas duas principais abordagens. Uma delas é baseada no estudo das doenças. As ciências ômicas (genômica, transcriptômica, proteômica ou metabolômica) são uma ferramenta muito utilizada, pois permitem realizar estudos de *screening*, diagnóstico, prognóstico, para o estudo da etiologia de diferentes doenças e para o descobrimento de biomarcadores específicos de uma doença (HORGAN; KENNY, 2011). A segunda abordagem consiste no desenvolvimento de dispositivos analíticos portáteis, fáceis de usar e rápidos que permitam detectar os biomarcadores específicos de uma doença. Esses dispositivos são conhecidos como biossensores. Segundo a IUPAC (MACNAUGHT; WILKINSON, 1997), um biossensor é um instrumento integrado capaz de fornecer uma informação específica quantitativa ou semiquantitativa, usando um elemento de reconhecimento biológico (receptor químico) que está em contato direto com o elemento de transdução.

Dentre todos os tipos de biossensores, aqueles baseados em transdutores eletroquímicos têm sido muito utilizados devido ao baixo custo, à facilidade de uso e a possibilidade de produzir dispositivos pequenos, gerando dispositivos portáteis. Em geral, a configuração dos sistemas eletroquímicos consiste em três eletrodos: o eletrodo de trabalho, em que na sua superfície é imobilizado o receptor biológico; o eletrodo de referência; e o contra eletrodo. Os biossensores eletroquímicos são divididos em função de como é gerado o sinal elétrico. Assim, existem, entre outros, biossensores potenciométricos, que medem variações no potencial de circuito aberto do sistema; biossensores amperométricos, que medem mudanças na corrente do sistema devido à oxidação ou redução de espécies eletroativas na superfície do eletrodo; e biossensores impedimétricos, que medem as mudanças na impedância complexa do sistema (HAMMOND et al., 2016). Desses três, os biossensores impedimétricos podem ser usados em configurações *label-free* e apresentar elevada sensibilidade e baixo custo. Eles são baseados na espectroscopia de impedância eletroquímica (EIE) para monitorar as modificações na superfície do eletrodo de trabalho. É uma técnica usada desde o final dos anos 70, entretanto somente após os anos 2000 foi descoberto o seu potencial como técnica de diagnóstico.

A *espectroscopia de impedância* mede a resistência elétrica complexa (impedância) da interfase eletrodo-solução, aplicando uma pequena perturbação no potencial a certa frequência e medindo a corrente resultante. O processo é modelado pelo circuito elétrico equivalente de Randles-Ershler. Geralmente, cada modificação do eletrodo de trabalho vai ser monitorada pelo valor do elemento  $R_{ct}$  (resistência de transferência de carga) do circuito (DANIELS; POURMAND, 2007; HAMMOND et al., 2016; LISDAT; SCHÄFER, 2008; SANTOS; DAVIS; BUENO, 2014). A EIE é uma técnica muito usada devido a sua sensibilidade. Porém, alguns problemas experimentais que podem comprometer os resultados obtidos têm sido reportados. Bogomolova, et al. (2009) mostraram que a elevada sensibilidade da técnica em sistemas analíticos pode levar a inespecificidade e falsos positivos. Vogt, et al. (2016) reportaram o efeito destrutivo da solução de ferri/ferrocianeto sobre a superfície de ouro depois das medidas e afirmaram que isto poderia comprometer a reprodutibilidade do sistema. Outro elemento importante dos biossensores impedimétricos são as monocamadas auto-montadas ou *self-assembled monolayers* (SAMs), usadas para modificar a superfície do transdutor. As SAMs foram descobertas por Nuzzo e Allara (1983) e consistem em uma camada ordenada de moléculas organizadas de forma espontânea sobre uma superfície sólida, devido às forças intermoleculares (ULMAN, 1996; VERICAT; VELA; SALVAREZZA, 2005). Uma configuração muito usada em sistemas baseados em EIE é a superfície de ouro funcionalizada com moléculas de alcanotóis. Para conseguir uma boa organização sem defeitos as moléculas precisam de 12-16 horas, devem apresentar uma elevada pureza, a superfície deve ser o mais lisa possível e ter o comprimento certo (SIGMA-ALDRICH, 2006). Em sistemas baseados em transferência de carga, como em biossensores impedimétricos, é importante conseguir um bom recobrimento da superfície. Uma monocamada com defeitos ou *pinholes* permitiria a livre migração iônica e eletrônica, não teria o efeito de impedância e a sensibilidade e resposta analítica do sistema se perderia (BOUBOUR; LENNOX, 2000; LEE; LENNOX, 2007).

A *capacitância derivada da impedância eletroquímica ou a espectroscopia de capacitância eletroquímica (ECE)* pode ser a solução para os problemas experimentais dos sistemas baseados em EIE. ECE mede a capacitância interfacial da monocamada dielétrica do eletrodo e é obtida pela conversão da função da impedância complexa,  $Z^*$ , em capacitância complexa,  $C^*$ , seguindo a equação (1), onde  $\omega$  é a frequência angular e  $i$  é  $\sqrt{-1}$  (ORAZEM; TRIBOLLET, 2008).

$$C_{dl} = C_i + C_q \quad (1)$$

A capacitância eletroquímica ( $C_{dl}$ ) é o equivalente em escala nano da capacitância química ( $C$ ), quando o eletrodo está imerso em uma solução, como acontece nas medidas de EIS.  $C_{dl}$  é resultado da combinação da capacitância iônica ( $C_i$ ) e da capacitância quântica ( $C_q$ ). A capacitância iônica ou capacitância da dupla camada ( $C_{dl}$ ) é a capacitância resultante da camada iônica gerada sobre a superfície do eletrodo. Comparando com um capacitor clássico, a superfície do eletrodo seria uma das placas metálicas e a camada iônica a outra, separadas por nm. Em uma situação não faradaica ou faradaica com a sonda redox em solução (ex. ferroceno),  $C_{dl}$  é dominada pela  $C_i$ . Quando a sonda redox está confinada na superfície do eletrodo, no potencial formal da monocamada eletroativa,  $C_q$  apresenta maior contribuição na  $C_{dl}$  do que a  $C_i$ , pois  $C_q$  depende da densidade de estados da sonda redox da monocamada e da superfície metálica do eletrodo. Em biossensoriamento, as modificações da superfície do eletrodo vão mudar a densidade de estados ( $\Gamma$ ) da sonda redox e por tanto a capacitância quântica, enquanto a capacitância iônica (monitorada no potencial redox-out) é quase constante (LEHR et al., 2017). As modificações do sistema vão se monitorar usando a capacitância redox ( $C_r$ ), seguindo a equação (2), onde  $e$  é a carga elementar,  $\Gamma$  é a densidade de estados,  $k_B$  é a constante de Boltzmann,  $T$  é a temperatura absoluta e  $f$  é a função de Fermi-Dirac.

$$C_r = \frac{e^2 \Gamma}{k_B T} \quad (2)$$

*Nesse trabalho* apresenta-se uma análise crítica de um sistema baseado em EIE. Os problemas experimentais observados durante o desenvolvimento do biossensor foram estudados e analisados com diferentes técnicas para conhecer a causa dos problemas. Os resultados foram comparados com a abordagem baseada em ECE, usando uma monocamada eletroativa de peptídeo. Como prova de conceito, ambos os sistemas foram desenhados para a detecção da proteína interleucina-6 (IL-6). IL-6 é uma



glicoproteína de 26 kDa, que tem um importante papel no processo imune e está envolvida em funções homeostáticas e neuroendócrinas (BARTON, 1997).

*Para a construção dos biossensores* foi realizado um pré-tratamento da superfície dos eletrodos de ouro. Esse processo consistiu em um polimento mecânico com alumina (1  $\mu\text{m}$ , 0,3  $\mu\text{m}$  e 0,05  $\mu\text{m}$ ), voltametria de redissolução em NaOH 0,5 M (100 ciclos desde -1,7 V a -0,7 V a uma velocidade de 100 mV/s) e polimento eletroquímico realizando uma voltametria em H<sub>2</sub>SO<sub>4</sub> 0,5 M a 80°C (25 ciclos desde -0,2 V a 1,5 V a uma velocidade de 100 mV/s). Os eletrodos limpos foram imersos na solução de monocamada durante 16 horas, sendo MUA + 6-COH 1 mM [1:20] em etanol para os experimentos de EIE e peptídeo redox 2 mM em acetonitrila-água (1:1 (v/v)) para os experimentos de ECE. Após a formação da monocamada, a SAM foi ativada por 30 minutos com uma solução de EDC 0,4 M e NHS 0,1 M (1:1 (v/v)) para a imobilização do anticorpo. A solução de Ab 1  $\mu\text{M}$  foi preparada em PB pH 7,4 e incubada durante 1 hora. Depois, os grupos não ocupados pelo anticorpo foram bloqueados com BSA 0,1% em PB pH 7,4 durante 30 minutos. A estabilidade do sistema foi testada realizando imersões por 30 minutos em PB pH 7,4. Cada etapa foi caracterizada realizando medidas de CV e EIE. Após a estabilização do sistema foi feito um controle negativo com fetuina (concentração similar à maior concentração de analito usada), e as incubações com o *target* específico. As soluções de proteína foram preparadas em PB pH 7,4 e incubadas durante 30 minutos. Depois foram feitas as medidas de EIE.

*Parte experimental configuração EIE* O sistema EIE foi otimizado em termos de estabilidade e reprodutibilidade. Porém, não foi obtida uma resposta analítica para nenhuma das proteínas testadas (IL-6, CRP, CEA e HER2). Cada etapa envolvida na obtenção da resposta analítica foi estudada. A atividade analito-anticorpo das proteínas testadas no sistema EIE foi estudada por ELISA. Todos eles mostraram atividade, inclusive nas concentrações usadas no EIE. A imobilização do anticorpo foi verificada por QCM. Após a ativação da SAM,  $4,3 \cdot 10^{12}$  as moléculas de anticorpo imobilizaram. O anticorpo foi orientado modificando o protocolo, imobilizando a proteína A antes da imobilização do anticorpo e, mesmo assim, não foi obtida uma resposta analítica. Por último foi estudado o efeito da espessura da monocamada na sensibilidade do sistema, substituindo a monocamada de tióis por uma SAM de cisteína e novamente não foi obtida uma resposta analítica. A última hipótese proposta foi a presença de *pinholes* na monocamada. O estudo dos defeitos da monocamada foi feito usando o protocolo de

Lee e Lennox (2007) e de Boubour e Lennox (2000). Foi confirmada a presença de defeitos na monocamada, pela imobilização do 11-FcC e pelo ângulo de fase ( $\phi$ ) da medida não faradaica da monocamada. Esses defeitos podem ter sido os responsáveis pela falta de sensibilidade e de resposta analítica do sistema, pois existia livre migração eletrônica e iônica. Para resolver esse problema foi proposto o sistema baseado em ECE.

*Parte experimental configuração ECE* O sistema ECE usado foi similar ao reportado por Piccoli, et al. (2018). Este sistema consistiu em uma monocamada auto-organizada de um peptídeo redox (Fc-Glu-Ala-Ala-Cys) em que foi imobilizado o anticorpo antiIL-6. A estabilidade obtida e os valores de  $C_r$  da SAM e de cada etapa de funcionalização foi muito similar aos obtidos por Piccoli, et al. (2018). O sistema apresentou uma variação de 0,7% entre os três brancos realizados. Porém, apesar da estabilidade, quando foi testado com soluções de diferentes concentrações de proteína IL-6 não foi obtida uma resposta analítica. A IL-6 é a menor proteína testada em um sistema baseado em ECE pelo nosso grupo. Comparando os resultados de trabalhos já publicados pelo grupo é possível correlacionar o tamanho das proteínas e a variação da resposta relativa por década de target (*slope*) das curvas analíticas obtidas para cada proteína e, por tanto à sensibilidade do sistema. Um dos sistemas mais usados consistiu em uma monocamada de 16-MHDA e 11-FcC [1:1]. Ele foi usado para detectar as proteínas NS1 (CECCHETTO et al., 2017), CRP e anti  $\alpha$ -sync (FERNANDES et al., 2015), de 46 kDa, 118 kDa e 150 kDa, respectivamente. As curvas analíticas conseguidas apresentaram uma *slope* de 14 para o sistema NS1, 30 para o sistema CRP e 84 para o sistema anti  $\alpha$ -sync. A falta de resposta analítica do sistema ECE para a proteína IL-6 pode ser devida ao peso molecular desta proteína não ser suficiente para ser detectada. Além disso, a sensibilidade do sistema também depende da relação do peso molecular entre o receptor biológico e o analito, pois sistemas formados por um receptor biológico menor do que o analito apresentam maior sensibilidade. No sistema do anti  $\alpha$ -sync de Fernandes et al. (2015), por exemplo, o receptor foi a  $\alpha$ -sync, um receptor celular de 14,4 kDa foi o que apresentou maior sensibilidade. Essa relação também foi reportada por Piccoli, et al. (2018). Eles compararam a sensibilidade do mesmo sistema ECE (monocamada eletroativa de peptídeo) quando era usado um anticorpo como receptor biológico (150 kDa) e um aptâmero de DNA. O sistema funcionalizado com o aptâmero mostrou uma sensibilidade quase oito vezes maior do que o sistema com anticorpo. No

sistema para a proteína IL-6 deste trabalho, o receptor biológico foi o anti IL-6, quase seis vezes maior do que a proteína (26 kDa). Assim, a falta de sensibilidade do sistema pode ter sido influenciada pelo pequeno tamanho do analito usado e pela diferença de tamanho entre o receptor e o target.

*Parte experimental sistema sonda redox em solução e confinada na superfície:* De forma paralela foi estudado o efeito da amplificação de sinal observado no experimento do estudo dos defeitos da SAM, nas medidas faradaicas com sonda redox em solução e imobilizada na superfície. Para isso, três eletrodos foram funcionalizados com o peptídeo redox e foram feitas as medidas de EIE em soluções de diferentes concentrações de  $[\text{Fe}(\text{CN})_6]^{3-/4-}$  (0,1; 0,2; 0,3; 0,5; 1,0; 2,0 mM). Para entender o processo de transferência de carga, as medidas foram feitas em três potenciais diferentes, no potencial da monocamada eletroativa, 0,38 V; no potencial da sonda redox em solução, 0,22 V e no potencial de meia onda das duas sondas, 0,30 V. Foi analisada a variação de quatro variáveis do sistema: capacitância redox ( $C_r$ ), frequência de relaxação ( $k$ ), resistência do sistema ( $R_q$ ) e o inverso da capacitância redox ( $1/C_r$ ) ou energia do sistema (BUENO; FERNANDES; DAVIS, 2017). A presença das duas sondas redox aumentou a condutividade e a densidade de corrente do sistema. Também, aumentou a energia do sistema e a frequência de relaxação com o aumento da concentração da sonda redox em solução. A capacitância redox do sistema diminuiu, assim como a resistência. Em conclusão, foi observada a transformação de um sistema capacitivo (formado só pela sonda confinada na superfície do eletrodo), em um sistema resistivo na presença da sonda redox em solução. O aumento da condutividade e da densidade de corrente tem concordância com o efeito de amplificação de sinal observado em experimentos anteriores. Esses resultados são promissores e essa configuração pode ser uma boa ferramenta para sistemas muito resistivos ou com baixa sensibilidade.

# List of figures

<b>Figure 1</b> - Biosensor design scheme .....	27
<b>Figure 2</b> – Electrochemical impedance spectroscopy faradaic configuration characteristics. A) Representation of the alkanethiol SAM deposited on the gold electrode surface and the electron transfer between the solution and the electrode surface; B) Nyquist impedance plot; C) Equivalent circuit capable of modeling impedimetric biosensor data; where $R_s$ is the solution resistant; $C_m$ is the monolayer capacitance; $R_t$ the film resistance; $C_t$ the film capacitance; $R_{ct}$ is the redox charge transfer resistant; and $Z_w$ is the Warburg element. The region inside the dashed line corresponds with the non-faradaic system and the continuous line region with the faradaic .....	29
<b>Figure 3</b> - Electrochemical capacitance spectroscopy faradaic configuration characteristics. A) Representation of the redox SAM deposited on the gold electrode surface; B) Nyquist capacitance plot; C) Equivalent circuit capable of modeling impedimetric biosensor data; where $R_s$ is the solution resistant; $C_m$ is the monolayer capacitance; $R_t$ the film resistance; $C_t$ the film capacitance; $R_{ct}$ is the redox charge transfer resistant; and $C_r$ is the redox capacitance, used to monitored the modifications of the redox SAM electrode.....	32
<b>Figure 4</b> - Schematic representation of the electrochemical impedance approach for antigen-antibody interaction. ....	37
<b>Figure 5</b> - Nyquist plots of the monolayers tested on gold electrode by different spacer-linker proportion at the formal potential and frequency range 0.1 Hz – 1 MHz. (A) MUA. Active gold electrode area: 0.043 cm <sup>2</sup> .; (B) MUA + 6-COH [1:1]. Active gold electrode area: 0.05 cm <sup>2</sup> .; (C) [1:5]. Active gold electrode area: 0.042 cm <sup>2</sup> .; (D) [1:15]. Active gold electrode area: 0.043 cm <sup>2</sup> .; (E) [1:20]. Active gold electrode area: 0.047 cm <sup>2</sup> .; (F) [1:30]. Active gold electrode area: 0.04 cm <sup>2</sup> .....	40
<b>Figure 6</b> – Cyclic voltammetry, Nyquist and Bode plots of the electrode functionalization process. A) Cyclic voltamogram; B) Nyquist impedance plot ( $-Z''$ vs $Z'$ ); C) Bode plot for real impedance ( $Z'$ vs frequency); D) Bode plot for imaginary impedance ( $-Z''$ vs frequency) of SAM, EDC/NHS, antiIL-6, block and blanks measurements, in the disk gold electrode (from Metrohm), in 1 mM [Fe(CN) <sub>6</sub> ] <sup>3-/4-</sup> , using 0.5 M KNO <sub>3</sub> and 12 mM PB pH 7.4 as supporting electrolyte. Active gold electrode area: 0.047 cm <sup>2</sup> .....	42
<b>Figure 7</b> - Nyquist impedance plot ( $-Z''$ vs $Z'$ ) of 6 blanks measurements (B 1-6): B(1-3) EIS measurement after the first PB pH 7.4 incubation; B(4-6) EIS measurements after 30 min PB pH 7.4 incubation), in the disk gold electrode (from Metrohm), in 1 mM [Fe(CN) <sub>6</sub> ] <sup>3-/4-</sup> , using 0.5 M KNO <sub>3</sub> and 12 mM PB pH 7.4 as supporting electrolyte. Active gold electrode area: 0.047 cm <sup>2</sup> .....	43

<b>Figure 8</b> - Nyquist and Bode plots of the target recognition steps. A) Nyquist impedance plot ( $-Z''$ vs $Z'$ ); B) Bode plot for real impedance ( $Z'$ vs frequency); C) Bode plot for imaginary impedance ( $-Z''$ vs frequency) of blanks, negative control with fetuin and IL-6 solutions, in the disk electrode (from Metrohm), in 1 mM $[\text{Fe}(\text{CN})_6]^{3-/4-}$ , using 0.5 M $\text{KNO}_3$ and 12 mM PB pH 7.4 as supporting electrolyte. Active gold electrode area: 0.047 $\text{cm}^2$ .....	44
<b>Figure 9</b> - Relative variation caused by the blanks incubation and the protein solution for 3 different targets: CRP, HER2 and CEA.....	45
<b>Figure 10</b> - Characterization of the system construction by QCM. Graphs from top to bottom: EDC/NHS activation; antibody immobilization; and BSA blocking in the quartz crystal. For each procedure, I) signal stabilization with the solution solvent PB (in B and C) or Millipore water (in A); II) incubation with the reagent; III) signal stabilization with the solution solvent.....	47
<b>Figure 11</b> - Scheme of the distribution of the antibody on the thiolated SAM with and without protein A. A) Direct immobilization: ideal Ab organization when it is directly immobilized by the constant region; B) Direct immobilization: real Ab organization when it is directly immobilized; C) Indirect immobilization: expected organization of the Ab previously protein A immobilization.....	48
<b>Figure 12</b> - Nyquist and Bode plots of the target recognition steps using an electrode functionalized with protein A. A) Nyquist impedance plot ( $-Z''$ vs $Z'$ ); B) Bode plot for real impedance ( $Z'$ vs frequency); C) Bode plot for imaginary impedance ( $-Z''$ vs frequency) of blanks, negative control with fetuin and target solutions, in 1 mM $[\text{Fe}(\text{CN})_6]^{3-/4-}$ , using 0.5 M $\text{KNO}_3$ and 12 mM PB pH 7.4 as supporting electrolyte. Active gold electrode area: 0.05 $\text{cm}^2$ .....	49
<b>Figure 13</b> - Relative variation caused by the blanks incubation and the protein solutions, using protein A in the system. Target1 = 1 $\mu\text{g mL}^{-1}$ ; Target2 = 10 $\mu\text{g mL}^{-1}$ .....	49
<b>Figure 14</b> - QCM results of the cysteine based system. Graphs from top to bottom: Cysteine immobilization; EDC/NHS activation; antibody immobilization; and BSA blocking in the quartz crystal. For each procedure, I) signal stabilization with the solution solvent PB (in A, C and D) or Millipore water (in B); II) incubation with the reagent; III) signal stabilization with the solution solvent.....	51
<b>Figure 15</b> - Nyquist and Bode plots of the target recognition steps using an electrode functionalized with cysteine monolayer. A) Nyquist impedance plot ( $-Z''$ vs $Z'$ ); B) Bode plot for real impedance ( $Z'$ vs frequency); C) Bode plot for imaginary impedance ( $-Z''$ vs frequency) of blanks, negative control with fetuin and target solutions, in 1 mM $[\text{Fe}(\text{CN})_6]^{3-/4-}$ , using 0.5 M $\text{KNO}_3$ and 12 mM PB pH 7.4 as supporting electrolyte. Crystal geometric area: 154 $\text{mm}^2$ .....	52
<b>Figure 16</b> - Thiolated SAM distribution on the gold electrode surface. A) Ideal distribution and behaviour of the functionalized electrode; B) hypothetical distribution of the SAM 1:20; C) hypothetical real distribution and deposition of the SAM 1:20 on the gold electrode surface.....	53

<b>Figure 17</b> - Faradaic and non-faradaic cyclic voltammogram of the bare gold and the [1:20] SAM in A) 1 mM $[\text{Fe}(\text{CN})_6]^{3-/4-}$ , using 0.5 M $\text{KNO}_3$ and 12 mM PB pH 7.4 as supporting electrolyte; B) 1 M $\text{NaClO}_4$ before and after 5 seconds incubation in 2 mM 11-FcC. Active gold electrode area: 0.05 $\text{cm}^2$ .....	54
<b>Figure 18</b> -Nyquist plots of the sequential SAM formation. A) Non-faradaic impedance Nyquist plot; B) Non-faradaic capacitance Nyquist plot of 1 mM 6-COH and 1 mM MUA deposition in 0.5 M $\text{KNO}_3$ and 12 mM PB pH 7.4; C) Faradaic impedance Nyquist plot; D) Faradaic capacitance Nyquist plot of 1 mM 6-COH, 1 mM MUA and 2 mM 11-FcC deposition in 1 mM $[\text{Fe}(\text{CN})_6]^{3-/4-}$ , using 0.5 M $\text{KNO}_3$ and 12 mM PB pH 7.4. Active gold electrode area: 0.047 $\text{cm}^2$ .....	55
<b>Figure 19</b> - Faradaic and non-faradaic cyclic voltammogram of the bare gold and 6-COH, MUA and 11-FcC deposition, in A) 1 mM $[\text{Fe}(\text{CN})_6]^{3-/4-}$ , using 0.5 M $\text{KNO}_3$ and 12 mM PB pH 7.4 as supporting electrolyte; B) 0.5 M $\text{KNO}_3$ and 12 mM PB pH 7.4; C) 1 M $\text{NaClO}_4$ after and before 60s and 300s incubation with 2 mM 11-FcC solution. Active gold electrode area: 0.047 $\text{cm}^2$ .....	56
<b>Figure 20</b> - Study of the the phase angle ( $\theta$ ) of the SAM constructed in sequential as an analyses of the presence of pinholes.....	57
<b>Figure 21</b> - Redox peptide SAM stability. M1-9: nine consecutive EIS measurements of the electroactive film. Active gold electrode area: 0.045 $\text{cm}^2$ .....	59
<b>Figure 22</b> – Cyclic voltammogram, Nyquist and Bode plots of the ECS based electrode functionalization process. A) Cyclic voltammogram; B) Nyquist capacitance plot ( $-C''$ vs $C'$ ); C) Bode plot for real capacitance ( $C'$ vs frequency); D) Bode plot for imaginary capacitance ( $-C''$ vs frequency) of SAM, SAM at de redox-out potential, antiIL-6, block and blanks measurements in 20 mM TBA as supporting electrolyte. Active gold electrode area: 0.045 $\text{cm}^2$ .....	60
<b>Figure 23</b> - Study of the stability of the biosensor surface for the protein IL-6. B1-3: triplicate EIS measurements after 30 min immersion in PB. B4-6: triplicate EIS measurements after a second immersion in PB during 30 min. B7-9: triplicate EIS measurements a third immersion in PB for 30 min. Active gold electrode area: 0.045 $\text{cm}^2$ .....	61
<b>Figure 24</b> - Nyquist and Bode plots of the detection of the protein IL-6. A) Nyquist capacitance plot ( $-C''$ vs $C'$ ); B) Bode plot for real capacitance ( $C'$ vs frequency); C) Bode plot for imaginary capacitance ( $-C''$ vs frequency) in 20 mM TBA as supporting electrolyte. Active gold electrode area: 0.045 $\text{cm}^2$ .....	61
<b>Figure 25</b> - Nyquist impedance plot of the detection of the protein CRP from Piccoli, et al. ....	62
<b>Figure 26</b> - Cyclic voltammetry plots of redox peptide SAM and redox probe in solution. A) CV in $[\text{Fe}(\text{CN})_6]^{3-/4-}$ in 0.5 M $\text{KNO}_3$ and 12 mM PB, comparing to B) cyclic voltammetry of redox peptide-based SAM in 20 mM TBA; 20 mM TBA and 0.1 mM $[\text{Fe}(\text{CN})_6]^{3-/4-}$ ; and in 20 mM TBA after the measurements. In A) vertical reference	

represents the formal potential of the  $[\text{Fe}(\text{CN})_6]^{3-/4-}$  in 0.5 M  $\text{KNO}_3$  and 12 mM PB, 0.25 V (dotted line); in B) the vertical references show the formal potential of the confined redox probe (redox peptide SAM), 0.38 V *versus* Ag|AgCl 3M KCl (dashed line); of the redox probe in 20 mM TBA, 0.22 V *versus* Ag|AgCl 3M KCl (dotted line); and the half potential of both redox probe, 0.30 V *versus* Ag|AgCl 3M KCl (dash-dot line). Active gold electrode area: 0.045  $\text{cm}^2$  ..... 64

**Figure 27** - EIS measurement in 0.38 V *versus* Ag|AgCl 3M KCl of the redox peptide SAM and redox probe in solution. A) Impedance Nyquist impedance plot; B) Capacitance Nyquist plot; C) Bode plot of real impedance ( $Z'$ ); D) Bode plot of imaginary impedance ( $Z''$ ); E) Bode plot of real capacitance ( $C'$ ); F) Bode plot of imaginary capacitance ( $C''$ ). Active gold electrode area: 0.045  $\text{cm}^2$  ..... 65

**Figure 28** - EIS measurement in 0.30 V *versus* Ag|AgCl 3M KCl of the redox peptide SAM and redox probe in solution. A) Impedance Nyquist impedance plot; B) Capacitance Nyquist plot; C) Bode plot of real impedance ( $Z'$ ); D) Bode plot of imaginary impedance ( $Z''$ ); E) Bode plot of real capacitance ( $C'$ ); F) Bode plot of imaginary capacitance ( $C''$ ). Active gold electrode area: 0.045  $\text{cm}^2$  ..... 66

**Figure 29** - EIS measurement in 0.22 V *versus* Ag|AgCl 3M KCl of the redox peptide SAM and redox probe in solution. A) Impedance Nyquist impedance plot; B) Capacitance Nyquist plot; C) Bode plot of real impedance ( $Z'$ ); D) Bode plot of imaginary impedance ( $Z''$ ); E) Bode plot of real capacitance ( $C'$ ); F) Bode plot of imaginary capacitance ( $C''$ ). Active gold electrode area: 0.045  $\text{cm}^2$  ..... 67

**Figure 30** - Analysis of the variation of the variables involved on the charge transfer process of the system with both redox probe confined and in solution. A) Redox capacitance,  $C_r$ ; B) Inverse of the redox capacitance,  $1/C_r$ ; C) Resonance resistance,  $R_q$ ; D) Frequency of charge relaxation,  $k$ . For each plot: black= EIS measurements in 0.38 V; red= EIS measurements in 0.30 V; green= EIS measurements in 0.22 V ..... 68

## List of tables

<b>Table 1</b> - $R_{ct}$ values, stability and reproducibility of the different SAMs tested.....	39
<b>Table 2</b> - ELISA assay results. Absorbance values of the proteins tested. ....	45
<b>Table 3</b> - Variation values in % of the blanks and the proteins measurements in different proteins.....	45
<b>Table 4</b> - Absolute frequency variation, mass variation and number of molecules per $\text{cm}^{-2}$ of the QCM assay for the cysteine, antibody and BSA immobilization.....	52
<b>Table 5</b> - Correlation coefficients ( $r^2$ ) of the lineal regression showed in Figure 29 for each variable and each potential. ....	69



# List of abbreviations and symbols

11-FcC	11-ferrocenylundecacethiol
6-COH	6-mercapto-1-hexanol
Ab	Antibody
Ala	Alanine
anti-	Antibody
BSA	Bovine serum albumin
c	Theoretical QCM sensitivity coefficient
C'	Real componente of complex capacitance
C''	Imaginary componente of complex capacitance
C*	Complex capacitance
-	Electrochemical capacitance
C <sub>dl</sub>	Double layer capacitance
C <sub>e</sub>	Electrostatic capacitance
CEA	Carcinoembryonic antigen
C <sub>m</sub>	Monolayer capacitance
C <sub>q</sub>	Quantum capacitance
C <sub>r</sub>	Redox capacitance
CRP	C-reactive protein
C <sub>t</sub>	Target capacitance
CV	Cyclic voltammetry
Cys	Cysteine
e	Elementary charge
ECE	Espectroscopia de capacitância eletroquímica
ECS	Electrochemical capacitance spectroscopy
EDC	1-Ethyl-3-(3-dimethylaminopropyl) carbodiimide (EDC)

EIE	Espectroscopia de impedância eletroquímica
EIS	Electrochemical impedance spectroscopy
ELISA	Enzyme linked immunosorbent assay
Eq.	Equation
f	Fermi-Dirac function
F <sub>ab</sub>	Variable region of an antibody
F <sub>c</sub>	Constant region of an antibody
Fc	Ferrocenyl
FRA	Frequency response analysis
Glu	Glutamic acid
HER2	Human epidermal growth factor receptor 2
hPAP	Human prostatic acid phosphatase
HRP	Horseradish peroxidase
i	$\sqrt{\quad}$
IgG	Immunoglobulin G
IL-6	Interleukin-6
$\varphi$	Phase angle
k	Frequency
k <sub>B</sub>	Boltzman constant
LOD	Limit of detection
M <sub>m</sub>	Molecular mass
MUA	11-mercaptoundecanoic acid
N <sub>A</sub>	Avogadro's constant
NHS	N-Hydrosuccinimide
NS1	Non-structural protein 1
OPD	o-Phenylenediamine dihydrochloride
PB	Phosphate buffer

PBS-T	Phosphate buffered saline with Tween 20
PEG	Polyethylene glycol
QCM	Quartz crystal microbalance
$r^2$	Coefficient of regression
$R_{ct}$	Charge transfer resistance
$R_q$	Quantum resistance
$R_s$	Solution resistance
RSD	Relative standard deviation
$R_t$	Target resistance
SAM	Self-assembled monolayer
T	Absolute temperature
TBA	tetrabutylammonium bromide
$\omega$	Angular frequency
$Z'$	Real component of the complex impedance
$-Z''$	Imaginary component of the complex impedance
$Z^*$	Complex impedance
$Z_w$	Warburg element
$\alpha$ -sync	$\alpha$ -synuclein
$\Gamma$	Density-of-states
$\Delta m$	Mass variation
$\Delta E_p$	Different between oxidation and reduction potential
$\Delta f$	Frequency variation

# Summary

<b>1. Introduction</b> .....	<b>27</b>
1.1. <i>Electrochemical impedance spectroscopy (EIS)</i> .....	28
1.2. <i>Electrochemical capacitance spectroscopy (ECS)</i> .....	31
<b>2. Objective</b> .....	<b>34</b>
<b>3. Experimental</b> .....	<b>34</b>
3.1. <i>Material, reagents and apparatus</i> .....	34
3.2. <i>Electrode surface pre-treatment</i> .....	35
3.3. <i>Electrochemical measurements</i> .....	35
3.4. <i>Gold electrode functionalization</i> .....	36
3.5. <i>Antigen-antibody interaction</i> .....	37
3.6. <i>Enzyme Linked Immunosorbent Assay (ELISA)</i> .....	37
3.7. <i>Quartz Crystal Microbalance (QCM) assays</i> .....	38
<b>4. Results and discussions</b> .....	<b>39</b>
4.1. <i>Self-assembled monolayer optimization</i> .....	39
4.2. <i>Faradaic electrochemical impedance spectroscopy assay</i> .....	40
4.3. <i>Study of the pair antigen-antibody activity</i> .....	44
4.4. <i>Study of the antibody immobilization step</i> .....	46
4.5. <i>Oriented-Ab-immobilization with protein A</i> .....	48
4.6. <i>Simultaneous QCM and EIS assay with cysteine monolayer</i> .....	50
4.7. <i>Study of the MUA + 6-COH 1:20 self-assembled monolayer defects</i> .....	53
4.8. <i>Faradaic impedance-derived capacitance assay</i> .....	58
4.9. <i>Electrochemical analysis of an electroactive film based system with redox probe in solution</i> .....	63
<b>5. Conclusion</b> .....	<b>72</b>
<b>References</b> .....	<b>73</b>

## 1. Introduction

In the last decades, the development of fast and simple analytical methods for disease diagnostic is one of the principal challenges for clinical research. In this direction, two principal approaches are being developed. One of them is based on the diseases study. Omic sciences (genomics, transcriptomics, proteomics or metabolomics) have transformed the way to study cellular and molecular systems, becoming an important tool for screening, diagnosis, prognosis or understanding the aetiology of the diseases. Such strategy lend to discovery biomarkers of the disease (HORGAN; KENNY, 2011) (“characteristic that is objectively measured and evaluated as an indicator of normal biological processes, pathogenic processes, or pharmacologic responses to a therapeutic intervention”, according to the National Institutes of Health Biomarkers Definitions Working Group in 1998 (ATKINSON et al., 2001)). The second approach is the development of portable, nice handle and rapid analytical devices suitable for biomarker detection in the field. These devices, called biosensors, are a self-contained integrated which are capable of providing specific quantitative or semiquantitative analytical information using a biological recognition element (biochemical receptor) which is in direct spatial contact with a transduction element, according to IUPAC (MACNAUGHT; WILKINSON, 1997) (Figure 1).

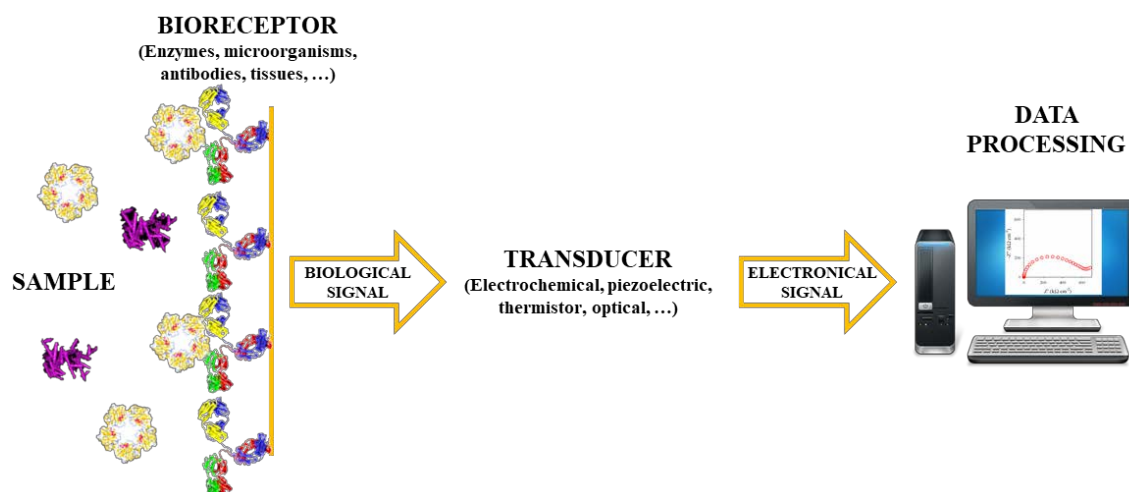


Figure 1 - Biosensor design scheme.

Source: Author

Among different biosensors, those based on electrochemical transducers (the biorecognition generates an electrical signal) are widely used, because they are low-cost and easy-to-use; and they can be miniaturized and portable, essential characteristics of biosensors. In general, those biosensors are constituted by a three-electrode system: a working or sensing electrode, whose

surfaces is modified with the bioreceptor; a reference electrode; and a counter electrode (HAMMOND et al., 2016). Electrochemical biosensors are divided according to how the electrical signal is generated. Some examples are potentiometric, amperometric or impedimetric.

Potentiometric biosensors usually measure variations in the open circuit potential of the system. The first potentiometric biosensor was described in 1969 by Guilbault and Montalvo (1969). It was an enzyme biosensor for the detection of urea in body fluids. It was based on the immobilization of the enzyme urease on an ammonia electrode. In the presence of urea, the enzyme catalysed its decomposition to ammonium ion, detectable by the ammonia electrode. Although potentiometric is an inexpensive, well-known technique, it shows worse analytical characteristics than using an amperometric transducer (KONCKI, 2007). Amperometric biosensors measure changes in current due to the oxidation or reduction of species on the electrode surface. Clark and Lyons (1962) developed the first amperometric-enzyme biosensor for glucose determination. Since then, numerous strategies have been published, most of them label-based. For analytical purposes, both methodologies require a tag, as a secondary antibody, an enzyme or a redox label (SANTOS; DAVIS; BUENO, 2014). Label-based configurations show disadvantages comparing with label-free techniques, since they need additional steps due to the process of labelling, so they are more laborious and time-consuming strategies. Label-free configurations bypass the label step, reduce the experimental time required and determine interactions in real-time (RAY; MEHTA; SRIVASTAVA, 2010). Potentiometric and amperometric transducers do not present the selectivity and sensitivity required by a label-free system. On the other hand, impedimetric biosensors have the potential for a label-free detection with high sensitivity and low cost.

### *1.1. Electrochemical impedance spectroscopy (EIS)*

It measures the system complex impedance ( $Z^*$ ) in every electrode surface modification. These biosensors use electrochemical impedance spectroscopy (EIS) to monitor each immobilization event on the electrode surface. This technique has been used since the late 1970s in corrosion studies, battery construction and in studies about charge transport across membranes. Its potential in diagnostics was discovered in the 2000s (DANIELS; POURMAND, 2007; LISDAT; SCHÄFER, 2008; ORAZEM; TRIBOLLET, 2008). Since then, more than 2000 works have been published, according with Pubmed. Most of them are based on a faradaic configuration with redox probe in solution (Figure 2A). EIS measures the complex electrical resistance (impedance) of the electrode-solution interface by applying a

small sinusoidal voltage at certain (and controllably varied) frequency and measuring the resulting current. Figure 2B shows the typical Nyquist impedance plot obtained. The process can be modeled by the Randles-Ershler electrical equivalent circuit (Figure 2C) and the  $R_{ct}$  element (charge transfer resistance) is used for monitor the surface modifications, since each variation of the surface changes the electron transfer process between the redox probe in solution and the electrode surface. Thus,  $R_{ct}$  value changes proportionally to the target concentration, achieving a high sensitivity (it have been reported limit of detection (LOD) in order of  $\text{pg mL}^{-1}$ ) (BAHADIR; SEZGINTÜRK, 2016; SANTOS; DAVIS; BUENO, 2014).

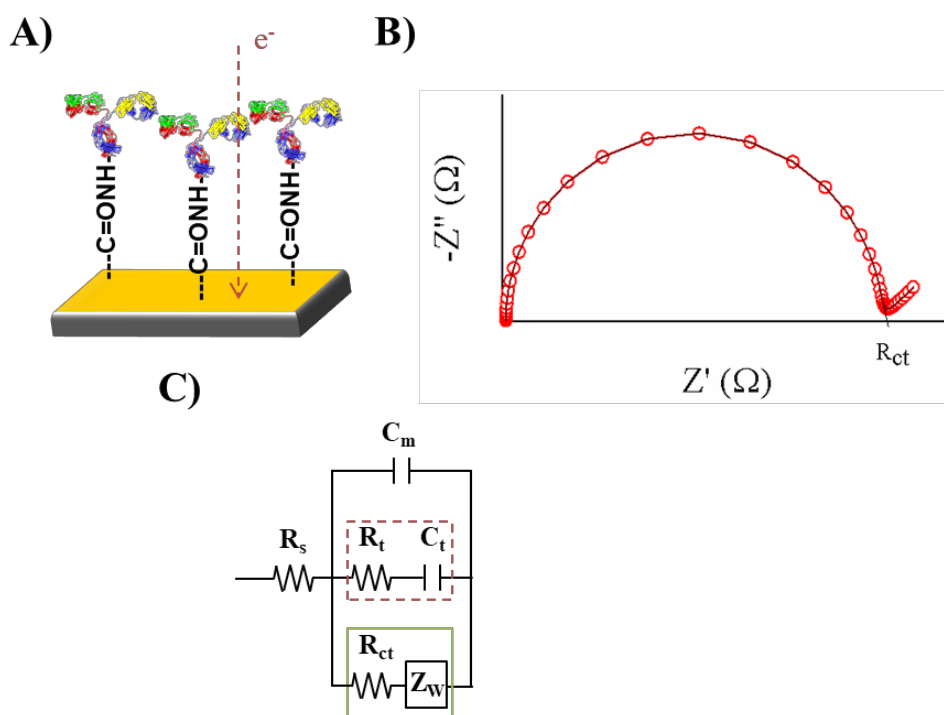


Figure 2 – Electrochemical impedance spectroscopy faradaic configuration characteristics. A) Representation of the alkanethiol SAM deposited on the gold electrode surface and the electron transfer between the solution and the electrode surface; B) Nyquist impedance plot; C) Equivalent circuit capable of modeling impedimetric biosensor data; where  $R_s$  is the solution resistant;  $C_m$  is the monolayer capacitance;  $R_t$  the film resistance;  $C_t$  the film capacitance;  $R_{ct}$  is the redox charge transfer resistant; and  $Z_w$  is the Warburg element. The region inside the dashed line corresponds with the non-faradaic system and the continuous line region with the faradaic.

Source: Author

In our group, some work have been published showing the potential of EIS in biosensing (CECCHETTO et al., 2015; FERNANDES et al., 2014) Both consisted in an immunosensor (antibody as a bioreceptor), faradaic system with redox probe (potassium ferri/ferrocyanide) in solution. Cecchetto, et al. (2015) developed a system based in an alkanethiol SAM for NS1 detection. They achieved a sensitivity of 14.1 percentage of variation per decade of protein (LOD of  $3 \text{ ng mL}^{-1}$ ). Fernandes, et al. (FERNANDES et al., 2014) reported an EIS system for

the detection of the protein CRP, achieving a limit of detection (LOD) of 0.264 nmol L<sup>-1</sup>. Although EIS has been proved to be an interesting technique for biosensing, it shows some experimental problems, as it is presented in this report. Sensitivity is the principal reason that makes EIS so popular. However, it can be a drawback, as was reported by Bogomolova et al. (2009) high sensitivity can be correlated with unspecific or false positive response. They described some factors that can change impedance without specific receptor – target interaction, such as initial electrode contamination (non-cleaned surface), repetitive EIS or CV measurements or immersions in the measurements buffer between measurements. Another drawback of the faradaic EIS system is the surface destruction by the [Fe(CN)<sub>6</sub>]<sup>3-/4-</sup> solution. Vogt et al. (2016) reported that measurements in ferri/ferrocyanide solution damage the electrode surface by the free CN<sup>-</sup> ions. Thus, after each measurement the surface changes and reproducible EIS measurements are not possible, even at the bare gold. This would be in agreement with the Bogomolova et al. observations. Notice that it was difficult to find references at the literature about the experimental difficulties. Those problems could compromise the reproducibility and sensitivity of the EIS based systems.

Commonly, in impedimetric biosensors the transducer surface is modified by a self-assembled monolayer (SAM) of alkanethiols, where is immobilised the specific biological receptor of the target of interest, usually an antibody. Self-assembled monolayers (SAMs) are organized single-molecule-thick films, based on a group of molecules spontaneously immobilized in an ordered and oriented way in a solid surface by intermolecular forces (ULMAN, 1996; VERICAT; VELA; SALVAREZZA, 2005). Since it was discovered by Nuzzo and Allara in 1983 (1983) that alkanethiols molecules had the ability to autoassembled spontaneously on noble metal surfaces, it constituted a versatile tool for creating surfaces with different chemical characteristic, since the head functional groups of the alkanethiols can be modified, thus the chemical properties of the SAM, enabling interactions with adjacent molecules or analytes. Those properties made SAMs an interesting element for biosensing. Alkanethiols have shown the ability to assembled on metal (Au, Pt, etc.), semiconductors or in oxide surfaces (SMITH; LEWIS; WEISS, 2004). In impedimetric biosensor it is widely used gold surfaces. The self-assembled of alkanethiols on a gold surface is governed by the combination of two driving forces. The first is the affinity that the sulphur groups present for gold, creating a stable and semi-covalent bond. The second driving forces are the van der Waals interactions between the methylene groups from the alkanethiols structures. The molecules immobilization and surface coverage is a very fast process, in the order of seconds or minutes. However, the monolayer requires more time (from 12 hours to 2 days) to get ordered and decrease the



uncovered defects (SIGMA-ALDRICH, 2006). Those defects can be caused by the purity of the alkanethiol used, the surface roughness and the length of the molecules. As was reported by Lee and Lennox, coverage defects in thiol-based SAMs are an important issue in system based on electron transfer process with redox probe in solution, such as EIS systems, where the electronic and ionic migration would be possible and the insulating properties of the SAM would be compromised (BOUBOUR; LENNOX, 2000; LEE; LENNOX, 2007). Those experimental issues were observed and studied in this work.

### 1.2. Electrochemical capacitance spectroscopy (ECS)

As was mentioned above, impedimetric biosensor could show some experimental problems that could compromised the reproducibility and sensitivity of the system. Thus, EIS could not be the best technique for biosensing. Here is proposed the impedance-derived capacitance or electrochemical capacitance spectroscopy (ECS) approach as a better alternative. ECS measures the interfacial capacitance of the electrode dielectric monolayer and is calculated by  $C^*$  obtained by conversion the impedance complex function  $Z^*$  (composed of real,  $Z'$ , and imaginary,  $Z''$ , components) from the EIS measurement, using the Eq. (1), wherein  $\omega$  is the angular frequency and is  $\sqrt{\omega}$  (ORAZEM; TRIBOLLET, 2008)

$$C^* = \frac{Z''}{\omega} \quad (1)$$

The electrochemical capacitance ( $C^*$ ) is the nanoscale equivalent of the chemical capacitance ( $C_{\mu}$ ) when the electrode is embedded into an electrolyte, such as in the EIS measurements.  $C^*$  is constituted by the combination of the ionic capacitance ( $C_i$ ) and the quantum capacitance ( $C_q$ ), following the Eq. (2). The ionic capacitance or double layer capacitance ( $C_{dl}$ ) is the resultant capacitance of the ion layer generated on the electrode surface, so, comparing with a classic capacitor, the electrode surface is one metallic plate and the ion layer is the other, separated by nm. In a non-faradaic situation or faradaic with redox probe in solution,  $C^*$  would be governed by the ionic capacitance. When the redox probe is confined on the electrode surface, a *pseudo-capacitance* is observed. In this case, at the formal potential the quantum capacitance has a higher contribution in the  $C^*$  value than the  $C_i$ , since  $C_q$  depends on the density-of-states of the confined redox probe and the metallic electrode surface.

$$\dots \dots \dots \quad (2)$$

For biosensing, the electrodes modifications alter the density-of-state ( $\Gamma$ ) of the redox probe, and so the  $C_q$  value, while the  $C_i$  value (monitored at the redox-out potential) would be almost constant (LEHR et al., 2017). Surface modifications are monitored by the redox capacitance ( $C_r$ ), following the Eq. (3), wherein  $e$  is the elementary charge,  $\Gamma$  is the density-of-states,  $k_B$  is the Boltzmann constant,  $T$  is the absolute temperature and  $f$  is the Fermi Dirac function.  $C_r$  would be maximized when (half of the available sites are occupied and half do not). This occurs at the half wave potential of the system, at which the measurements are performed. Experimentally,  $C_r$  corresponds with the diameter of the semicircle obtained after the measurement (Figure 3B). It is modeled by a derived Randles-Ershler circuit, showed in Figure 3C.

$$\dots \dots \dots \quad (3)$$

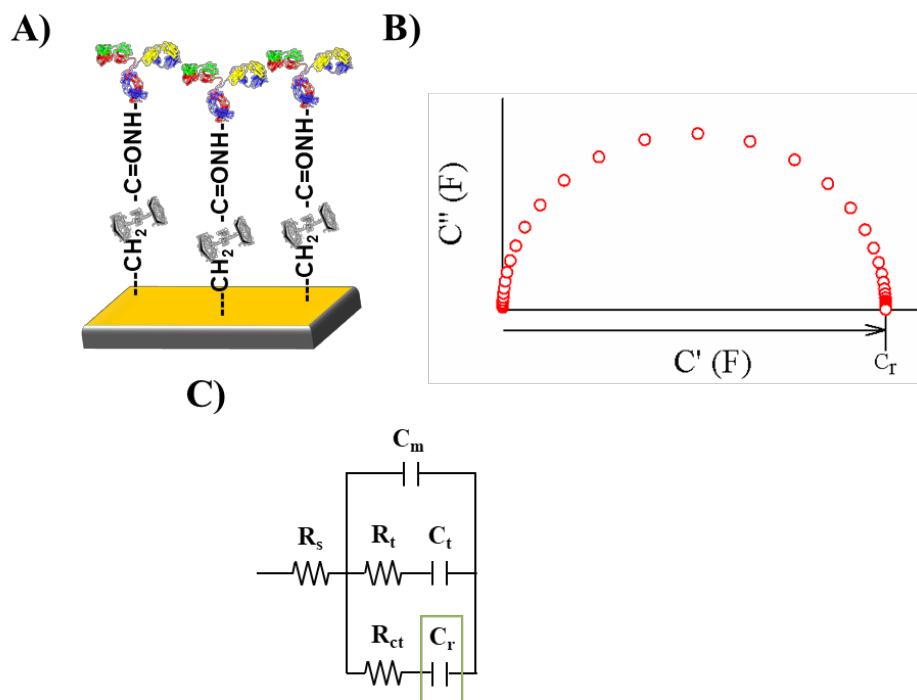


Figure 3 - Electrochemical capacitance spectroscopy faradaic configuration characteristics. A) Representation of the redox SAM deposited on the gold electrode surface; B) Nyquist capacitance plot; C) Equivalent circuit capable of modeling impedimetric biosensor data; where  $R_s$  is the solution resistant;  $C_m$  is the monolayer capacitance;  $R_t$  the film resistance;  $C_t$  the film capacitance;  $R_{ct}$  is the redox charge transfer resistant; and  $C_r$  is the redox capacitance, used to monitored the modifications of the redox SAM electrode.

Source: Author

The potential of ECS in biosensing have been widely studied and proved by our group. Fernandes, et al. developed a ECS-based biosensor for  $\alpha$ -sync and CRP, using a thiolated redox SAM with 11-ferrocenyl-undecanethiol (11-FcC) (FERNANDES et al., 2015). Cecchetto, et al. applied the same system as that reported by Fernandes, et al. (2015) for NS1 detection and compared it with the EIS configuration. They showed a limit of detection (LOD) 15 times lower using the ECS configuration instead of the EIS (CECCHETTO et al., 2017). The protein hPAP (human prostatic acid phosphatase) was also detected, using an ECS system by Fernandes, et al. (2017). They used a SAM composed by PEG (polyethylene glycol) and 11-FcC [1:99] and achieved a LOD of  $4.1 \pm 1.3$  pM. That same self-assembled monolayer was used by Santos, et al. (2018) for the detection of two biomarkers for dengue diagnostic (NS1 and IgG levels). The achieved sensitivities (percentage of signal variation per decade of protein concentration) were 4.5 for NS1 and 6.3 for IgG. Other redox surfaces non-based on 11-FcC were tested too. Redox peptide-based electroactive SAMs show advantages over redox alkanethiolated SAMs, such as peptide are easily manipulated and they can be designed to be the receptor of specific target (AMBLARD et al., 2006). Santos, et al. used an electroactive peptide SAM for CRP detection, showing a limit of detection of  $94 \text{ ng mL}^{-1}$  (SANTOS et al., 2015). The capacity of self-assembled and its utility in ECS system were tested with different peptides, as was reported by Piccoli, et al. (2016).

Here, a critical analysis for the EIS approach is presented. A mix thiol-based self-assembled monolayer was chemisorbed on the electrode surface for protein detection by EIS. The experimental problems observed during this objective were deeply studied using different techniques, such as QCM and ELISA, and by faradaic and non-faradaic strategies. Those result were compared with the faradaic ECS approach, using an electroactive peptide based SAM, in terms of sensitivity and reproducibility. As a proof of concepts, the systems (both EIS and ECS configuration) were designed for the detection of the protein interleukin 6 (IL-6). Human IL-6 is a 26 kDa glycoprotein, member of the cytokines family. It has an important role in immune process and it is involved in homeostatic and neuroendocrine functions (BARTON, 1997).

## 5. Conclusion

A stable and quite reproducible impedimetric device was achieved. During the first part of the work, each step of the functionalization process was studied and evaluated. It was demonstrated the interaction between the antibody and the antigen by ELISA; the antibody immobilization on the modified electrode by QCM; and its orientation was controlled by protein A. However, not analytical response was achieved. The ferrocenylalkylthiol system from Lee and Lennox (LEE; LENNOX, 2007) suggested the presence of coverage defects (pinholes) on the thiolated monolayer. Those pinholes could be the reason of the absence of specific response. They would allow the redox couple to access freely the electrode surface, so the impedimetric phenomenon would not be effective. As a solution, ECS with an electroactive SAM was proposed, because the contributions of the non-faradaic processes (such as the SAM defects) to the system capacitance are lower than that due to the surface modifications, associated with the formal potential of the system. Nevertheless, it was not achieved an analytical response system for protein IL-6. Previous work based on ECS showed analytical curves for different proteins. This is the first time that ECS is used to detect the protein IL-6 and it is smaller than the protein already used previously by our group. Comparing the results of same ECS system (same SAM) used to detect different proteins, it was possible to correlate the molecular weight of the target and the receptor with the sensitivity of the system. According to that, the absence of response in the ECS system proposed here for IL-6 detection was associated to the molecular weight of the protein IL-6 (26 kDa). It was not considered big enough to be detected by the redox peptide based ECS system. Finally, it was studied the behaviour of a system with two redox probes (attached and in solution). It was observed the variation from a capacitive-based system, when only the confined redox probe was involved, to an impedance one, when the redox probe in solution was present. The presence of the two redox probes increased the current density and the energy of the system. The frequency of charge relaxation ( $k$ ) increased with the increase of the redox probe in solution concentration and the redox capacitance ( $C_r$ ) decreased. Those results showed that the two-redox probe configuration could be a signal amplifier system. It could be a good tool for high resistive systems and/or low sensitive systems.

In conclusion, the EIS and ECS electroanalytical techniques are widely used in biosensing, since they show high sensitivity. However, they need an accurate control of the system design, in terms of the surface chemistry and the biosensing interface, in order to achieved specific detection.

## References

- AMBLARD, M. et al. Methods and protocols of modern solid phase peptide synthesis. **Molecular Biotechnology**, v. 33, n. 3, p. 239–254, 2006.
- ATKINSON, A. J. et al. Biomarkers and surrogate endpoints: Preferred definitions and conceptual framework. **Clinical Pharmacology and Therapeutics**, v. 69, n. 3, p. 89–95, 2001.
- BAHADIR, E. B.; SEZGINTÜRK, M. K. A review on impedimetric biosensors. **Artificial Cells, Nanomedicine, and Biotechnology**, v. 44, n. 1, p. 248–262, 2016.
- BARD, A. J.; FAULKNER, LARRY, R. **Electrochemical Methods: Fundamentals and applications**. 2nd. ed. New York: John Wiley & Sons, 2000.
- BARTON, B. E. IL-6: Insights into novel biological activities. **Clinical Immunology and Immunopathology**, v. 85, n. 1, p. 16–20, 1997.
- BOGOMOLOVA, A. et al. Challenges of electrochemical impedance spectroscopy in protein biosensing challenges of electrochemical impedance spectroscopy in protein biosensing. **Analytical Chemistry**, v. 81, n. 10, p. 3944–3949, 2009.
- BOUBOUR, E.; LENNOX, R. B. Insulating properties of self-assembled monolayers monitored by impedance spectroscopy. **Langmuir**, v. 16, n. 9, p. 4222–4228, 2000.
- BUENO, P. R.; FERNANDES, F. C. B.; DAVIS, J. J. Quantum capacitance as a reagentless molecular sensing element. **Nanoscale**, v. 9, p. 15362–15370, 2017.
- CECCHETTO, J. et al. An impedimetric biosensor to test neat serum for dengue diagnosis. **Sensors and Actuators, B: Chemical**, v. 213, p. 150–154, 2015.
- CECCHETTO, J. et al. The capacitive sensing of NS1 Flavivirus biomarker. **Biosensors and Bioelectronics**, v. 87, n. June 2016, p. 949–956, 2017.
- CLARK, L. C.; LYONS, C. Electrode systems for continuous monitoring in cardiovascular surgery. **Annals Of The New York Academy Of Sciences**, v. 102, n. 1, p. 29–45, 1962.
- DANIELS, J. S.; POURMAND, N. Label-free impedance biosensors: opportunities and challenges. **Electroanalysis**, v. 19, n. 12, p. 1239–1257, 2007.
- FERNANDES, F. C. B. et al. Comparing label free electrochemical impedimetric and capacitive biosensing architectures. **Biosensors and Bioelectronics**, v. 57, p. 96–102, 2014.
- FERNANDES, F. C. B. et al. Optimized diagnostic assays based on redox tagged bioreceptive interfaces. **Analytical Chemistry**, v. 87, n. 24, p. 12137–12144, 2015.
- FERNANDES, F. C. B.; BUENO, P. R. Optimized electrochemical biosensor for human prostatic acid phosphatase. **Sensors and Actuators, B: Chemical**, v. 253, p. 1106–1112, 2017.
- FISCHER, L. M. et al. Gold cleaning methods for electrochemical detection applications. **Microelectronic Engineering**, v. 86, n. 4–6, p. 1282–1285, 2009.
- GUILBAULT, G. G.; MONTALVO, J. G. A urea-specific enzyme electrode. **Journal of the American Chemical Society**, v. 91, n. 8, p. 2164–2165, 1969.
- HAMMOND, J. L. et al. Electrochemical biosensors and nanobiosensors. **Essays in Biochemistry**, v. 60, n. 1, p. 69–80, 2016.
- HERMANSON, G. T. Bioconjugate Reagents. **Bioconjugate Techniques**, p. 214–233, 2008.

- HORGAN, R. P.; KENNY, L. C. SAC review “Omic” technologies : proteomics and metabolomics. **The Obstetrician & Gynaecologist**, v. 13, p. 189–195, 2011.
- KIECOLT-GLASER, J. et al. Chronic stress and age-related increases in the proinflammatory cytokine IL-6. **Proceedings of the National Academy of Sciences of the United States of America**, v. 100, n. 15, p. 9090–9095, 2003.
- KONCKI, R. Recent developments in potentiometric biosensors for biomedical analysis. **Analytica Chimica Acta**, v. 599, n. 1, p. 7–15, 2007.
- LANGONE, J. J. Protein A of *Staphylococcus aureus* and related immunoglobulin receptors produced by streptococci and pneumococci. **Advances in Immunology**, v. 32, p. 157–252, 1982.
- LEE, L. Y. S.; LENNOX, R. B. Ferrocenylalkylthiolate labeling of defects in alkylthiol self-assembled monolayers on gold. **Physical Chemistry Chemical Physics**, v. 9, n. 8, p. 1013–1020, 2007.
- LEHR, J. et al. Mapping the ionic fingerprints of molecular monolayers. **Physical Chemistry Chemical Physics**, v. 19, n. 23, p. 15098–15109, 2017.
- LISDAT, F.; SCHÄFER, D. The use of electrochemical impedance spectroscopy for biosensing. **Analytical and Bioanalytical Chemistry**, v. 391, n. 5, p. 1555–1567, 2008.
- MACNAUGHT, A. D.; WILKINSON, A. **IUPAC. Compendium of Chemical Terminology, 2nd ed. (the “Gold Book”)**. Disponível em: <<https://goldbook.iupac.org/html/B/B00663.html>>. Acesso em: 8 maio. 2017.
- NUZZO, R. G.; ALLARA, D. L. Adsorption of bifunctional organic disulfides on gold surfaces. **Journal of the American Chemical Society**, v. 105, n. 13, p. 4481–4483, 1983.
- ORAZEM, M. E.; TRIBOLLET, B. **Electrochemical Impedance Spectroscopy**. Hoboken, NJ, USA: John Wiley & Sons, 2008.
- PICCOLI, J. et al. Redox capacitive assaying of C-reactive protein at a peptide supported aptamer interface. **Analytical Chemistry**, v. 90, n. 5, p. 3005–3008, 2018.
- PICCOLI, J. P. et al. The self-assembly of redox active peptides: Synthesis and electrochemical capacitive behavior. **Biopolymers**, v. 106, n. 3, p. 357–367, 2016.
- RAY, S.; MEHTA, G.; SRIVASTAVA, S. Label-free detection techniques for protein microarrays: Prospects, merits and challenges. **Proteomics**, v. 10, n. 4, p. 731–748, 2010.
- SAENGER, W. Structure and dynamics of water surrounding biomolecules. **Annual Review of Biophysics and Biomolecular Structure**, v. 16, n. 1, p. 93–114, 1987.
- SANTOS, A. et al. Redox-tagged peptide for capacitive diagnostic assays. **Biosensors and Bioelectronics**, v. 68, p. 281–287, 2015.
- SANTOS, A.; BUENO, P. R.; DAVIS, J. J. A dual marker label free electrochemical assay for Flavivirus dengue diagnosis. **Biosensors and Bioelectronics**, v. 100, n. September 2017, p. 519–525, 2018.
- SANTOS, A.; DAVIS, J. J.; BUENO, P. R. Fundamentals and applications of impedimetric and redox capacitive biosensors. **Journal of Analytical & Bioanalytical Techniques**, v. S7, n. 12, 2014.
- SAUERBREY, G. Z. Z. Verwendung von schwingquarzen zur wägung dünner schichten und

zur mikrowägung. **Zeitschrift für Physik**, v. 115, p. 206–222, 1959.

SIGMA-ALDRICH. Molecular Self-Assembly. **Material Matters**, v. 1, n. 2, p. 1–19, 2006.

SIMÃO, E. P. et al. Biosensor based on cysteine monolayer and monoclonal antibody for specific detection of aflatoxin b1 in rice. **Journal of the Brazilian Chemical Society**, v. 27, n. 6, p. 1040–1047, 2016.

SMITH, R. K.; LEWIS, P. A.; WEISS, P. S. Patterning self-assembled monolayers. **Progress in Surface Science**, v. 75, n. 1–2, p. 1–68, 2004.

THERMO SCIENTIFIC. ELISA technical guide and protocols. **Thermo Scientific**, v. 65, n. 815, p. 1–14, 2010.

TRASATTI, S.; PETRII, O. A. Real surface area measurements in electrochemistry. **Pure and Applied Chemistry**, v. 63, n. 5, p. 711–734, 1991.

ULMAN, A. Formation and structure of self-assembled monolayers. **Chemical Reviews**, v. 96, n. 4, p. 1533–1554, 1996.

VERICAT, C.; VELA, M. E.; SALVAREZZA, R. C. Self-assembled monolayers of alkanethiols on Au(111): Surface structures, defects and dynamics. **Physical Chemistry Chemical Physics**, v. 7, n. 18, p. 3258, 2005.

VOGT, S. et al. Critical view on electrochemical impedance spectroscopy using the ferri/ferrocyanide redox couple at gold electrodes. **Analytical Chemistry**, v. 88, n. 8, p. 4383–4390, 2016.